A Novel Imaging Approach for Early Detection of Prostate Cancer Based on Endogenous Zinc Sensing

Subrata K. Ghosh[1]
Pilhan Kim[3]
Xiao-an Zhang[2]
Seok-Hyun Yun[3]
Anna Moore[1*]
Stephen J. Lippard[2*§]
Zdravka Medarova[1#*§]

[1] Molecular Imaging Laboratory, MGH/MIT/HMS Athinoula A. Martinos Center for Biomedical Imaging, Department of Radiology, Massachusetts General Hospital, Harvard Medical School, Boston MA 02129
[2] Department of Chemistry, Massachusetts Institute of Technology, Cambridge MA 02139
[3] Wellman Center for Photomedicine, Department of Dermatology, Massachusetts General Hospital, Harvard Medical School, Boston MA 02114

Running Title: Imaging Zinc in Prostate Cancer

Keywords: imaging, prostate, cancer, zinc

[#] Work at MIT was supported under grant GM065519 from the National Institute of General Medical Sciences. Work at the Martinos Center for Biomedical Imaging was supported under grant R00CA129070 from the National Cancer Institute. Work at the Wellman Center for Photomedicine was supported under grant RC1DK086242 from the National Institute of Diabetes and Digestive and Kidney Diseases and Tosteson Postdoctoral Fellowship.
[*] Address correspondence to:
Zdravka Medarova, Ph.D., Molecular Imaging Laboratory, MGH/MIT/HMS Athinoula A. Martinos Center for Biomedical Imaging, Department of Radiology, Massachusetts General Hospital/Harvard Medical School, Bldg.75, 13th St., Charlestown, Massachusetts 02129; Tel:(617)643-4889; Fax:(617)643-4865; E-mail:zmedarova@partners.org,
Stephen J. Lippard, Ph.D., Department of Chemistry, 18-498, Massachusetts Institute of Technology, Cambridge, MA 02139; Tel:(617)253-1892; Fax:(617)258-8150 ; E-mail:lippard@mit.edu, or
Anna Moore, Ph.D., Molecular Imaging Laboratory, MGH/MIT/HMS Athinoula A. Martinos Center for Biomedical Imaging, Department of Radiology, Massachusetts General Hospital, Bldg. 75, 13th St, Charlestown, MA 02129; Tel: (617)724-0540; Fax: (617)-643-4865; E-mail: amoore@helix.mgh.harvard.edu
[§] Authors contributed equally

Abstract

The early detection of prostate cancer is a life-saving event in patients harboring potentially aggressive disease. With the development of malignancy there is a dramatic reduction in the zinc content of prostate tissue associated with the inability of cancer cells to accumulate the ion. In the current study, we utilized endogenous zinc as an imaging biomarker for prostate cancer detection and progression monitoring. We employed a novel fluorescent sensor for mobile zinc (ZPP1) to detect and monitor the development of prostate cancer in a transgenic mouse model of prostate adenocarcinoma, using in vivo optical imaging correlated with biological fluid-based methods. We demonstrated that the progression of prostate cancer could be monitored in vivo judging by decreasing zinc content in the prostates of tumor-bearing mice in an age-dependent manner. In a novel quantitative assay, we determine the concentration of mobile zinc in both prostate cell lysates and mouse prostate extracts through simple titration of the ZPP1 sensor. Our findings fulfill the promise of zinc-based prostate cancer diagnostics with the prospect for immediate clinical translation.

Introduction

Prostate cancer is the second leading cause of cancer death in men, exceeded only by lung cancer (1) and causes no symptoms in its early curable stage. Consequently, the ability to diagnose prostate cancer early, before it has spread beyond the confines of the organ, could offer the only possibility of a cure to patients at risk for aggressive disease.

The current clinical diagnosis and staging of prostate cancer relies on four core parameters: digital rectal examination (DRE), serum prostate-specific antigen (PSA), biopsy, and imaging (2). However, all of these tests are associated with considerable shortcomings in terms of specificity, sensitivity, and/or invasiveness.

It has been widely accepted by the scientific community that elevated PSA levels do not necessarily signal the presence of cancer. Overall, only 30 percent of men with abnormal PSA levels have prostate cancer (3). The lack of reliable diagnostic and staging tools for prostate cancer leads to unnecessary invasive and emotionally taxing surgery or undiagnosed disease. Therefore, a true diagnostic biomarker is urgently needed.

Over half a century of research has identified mobile zinc as an excellent candidate biomarker for prostate cells. The healthy prostate contains the highest concentrations of mobile zinc of all soft tissues in the body. These levels decrease dramatically during the development of prostate cancer, in agreement with downregulation of the ZIP1 transporter in cancer cells (4), even at an early stage (5). Even more importantly, there is an abundance of evidence in the literature that prostate cancer is the *only* known disease of the prostate that displays such a substantial decrease in tissue zinc content and that neither prostatitis nor benign prostatic hyperplasia are associated with this phenotype (6, 7). Reportedly, the zinc concentration in the malignant

peripheral prostate, which is the main region of cancer development, is reduced six-fold compared to the normal peripheral prostate (500 vs. 3000 nmols/g). This difference is even more dramatic in prostatic fluid (1000 vs. 9000 nmols/g) (6). Furthermore, computer modeling studies, based on synthetic images produced from clinically measured zinc-concentration distributions, suggest that zinc-based diagnostics represents an approach superior to PSA in terms of sensitivity to the tumor grade, and detection capability for tumors with a Gleason score over 6. In addition, the amount of zinc depletion could be used as a measure of the Gleason score of the tumor (8, 9).

In the current study we report a novel method for early detection of prostate cancer based on zinc as a quantitative imaging biomarker. Using a new ditopic zinc sensor (ZPP1) with a unique biphasic response to the ion (10), we were able to image the progression of prostate cancer in vivo in the TRAMP mouse model, which was deemed most appropriate because it develops progressive prostate cancer that histopathologically mimics human disease. TRAMP mice recapitulate many salient aspects of human prostate cancer and have been utilized for a wide range of studies (11-18). By contrast, other models, for example those in which prostate cancer is driven by overexpression of *c-myc*, display a more modest phenotype and develop PIN, which progresses to invasive cancer over the course of 6-12 months (19). Furthermore, the progression of prostate cancer from well to poorly differentiated malignancy is not as sufficiently characterized in the relatively recent *c-myc* model, which is used primarily to study PIN, whereas the TRAMP model has been validated through many years of research (11-18).

In addition to our imaging studies, we took advantage of the turn-on fluorescence property of ZPP1 upon binding to precisely two molecules of zinc to quantify zinc in

tissue lysates and prostate cancer cell lines. These measurements offered us an accurate means to correlate our imaging data with native zinc tissue abundance. To our knowledge, this is the first study describing the use of zinc as an innate imaging biomarker in prostate cancer, which we believe will pave the way to a new quantitative method for early cancer detection.

Materials and Methods

Chemical Reagents

tris[(2-Pyridyl)methyl]amine, TPA, was purchased from ATRP Solutions Inc., USA, and used as received. The cell membrane-permeable fluorescent Zn^{2+} sensor ZPP1was prepared according to a literature procedure (10).

Cell Lines

Human prostate epithelial cell lines (RWPE1, RWPE2, LNCaP, and DU145) were authenticated based on viability, recovery, growth, morphology, and isoenzymology by the supplier (American Tissue Collection Center, ATCC, Manassas, VA). Culture conditions are described in Supplemental Data.

Fluorescence microscopy

The abundance of zinc in cultured cell lines was analyzed using fluorescence microscopy. Confocal microscopy was used to determine the cellular distribution of zinc and the relative expression of the ZIP1 transporter. Experimental details are provided in Supplemental Data.

Zinc quantification in prostate cells by flow cytometry

Zinc abundance in RWPE1 and RWPE2 cells was quantified by flow cytometry. Experimental details are provided in Supplemental Data.

Determination of zinc concentration using ZPP1 titration

Cell lines. Cells lines were incubated with $ZnCl_2$ for 18 h, detached using cell dissociation buffer (Gibco-BRL, Carlsbad, CA), resuspended in Hepes/KCl buffer (25 mM Hepes and 100 mM KCl, pH: 7.0), and stored at -80 °C for 24 h. The next day, the cells were thawed at room temperature and sonicated using 6-8 strokes at 4 °C. Then, 0.2

ml aliquots of the cell lysates were placed in 96-well plates for ZPP1 titration. Titration was performed as previously described (10). Briefly, ZPP1 was titrated into the sample to achieve step-wise increments in ZPP1 concentration. At each step, the fluorescence was measured (excitation 505 nm, emission 532 nm) using a SpectraMax M2 fluorescence spectrophotometer (Molecular Devices, Union City, CA). At each step, the fluorescence of buffer containing ZPP1 alone (no $ZnCl_2$) was subtracted from the lysate measurements. Zinc levels were divided by the number of cells used to make the lysate in order to obtain the zinc content per cell.

Prostate (Mouse) total extracts. Prostate extracts were prepared directly from excised prostate tissue by suspending the tissue in 2 ml of Hepes/KCl buffer and briefly homogenizing it, followed by storage at -80 °C. The tissue was thawed and sonicated using the procedure described for cell lysates. ZPP1 titration was performed as described for cell lysates.

In accord with the literature (10), initial validation experiments in cell lysates and prostatic extracts confirmed that ZPP1 concentration at the peak fluorescence equals half of the zinc concentration in the sample.

Inductively coupled plasma-mass spectrometry (ICP-MS)

Prostate extracts (200 µl) or prostate cell lysates (200 µl) were digested in concentrated HNO_3 (0.5 ml) overnight at 37 °C and analyzed for Zn^{2+} concentration by ICP-MS using added strontium as an internal control.

Animals

Male TRAMP (Transgenic Adenocarcinoma of the Mouse Prostate, C57BL/6-Tg(TRAMP)8247Ng/J) and control C57BL/6J mice (Jackson Laboratories; Bar Harbor,

ME; n = 8) were used in our experiments. A mouse model of inflammation was generated as described in (20). Briefly, animals were injected intraperitoneally with 1mg/kg of lipopolysaccharide (LPS, Sigma-Aldrich, St. Louis, MO). The animals were used in experiments 18 h after injection. All animal experiments were performed in compliance with institutional guidelines and approved by the Subcommittee on Research Animal Care (SRAC) at Massachusetts General Hospital.

Optical Imaging and Image Analysis

For optical imaging, animals were placed into a whole-body animal imaging system (IVIS Spectrum, Caliper Life Sciences, Hopkinton MA), equipped with a 500 nm excitation and a 540-nm emission filter. In the initial feasibility experiments, C57BL/6J mice were imaged by epifluorescence before and 30 min after tail-vein injection of either ZPP1 alone (100 µl of a 500 µM solution) or ZPP1 plus chelator (TPA; 5mM). The fluorescence imaging settings (exposure time: 0.5 sec., F-stop: 2; Binning: medium) were kept constant for comparative analysis. Gray scale white-light photographs and epifluorescent images were acquired, superimposed, and analyzed by using the Living Image software. Image analysis was performed by manually selecting a region of interest (ROI) overlying the prostate or muscle, as a control. The area of the ROI was kept constant and the intensity was recorded as average efficiency. To determine the origin of the observed signal, in a set of animals we also performed transillumination optical imaging with fluorescence imaging tomographic reconstruction, according to the manufacturer's protocol. In some experiments, after imaging, the animals were sacrificed and the prostate and muscle tissue removed and imaged ex vivo, using the same settings as for in vivo imaging. In the subsequent experiments, age-matched TRAMP and

C57BL/6J control mice were imaged at 15-, 19-, 24-, and 28-wks of age, using the settings established in the feasibility studies. At each time point, a set of animals was sacrificed, prostates removed, imaged ex vivo, and used for microscopy to determine disease stage and ZPP1 accumulation.

Intravital Microscopy

A home-built *in viv*o fluorescence confocal laser scanning microscopy system, as previously described (21), was utilized to monitor the uptake of ZPP1 by epithelial cells in the prostate of live mice. Mice were anaesthetized by an intraperitoneal injection of ketamine (80mg/kg) + xylazine (10mg/kg) and placed on the heated plate integrated to the XYZ motorized stage. Prior to imaging, ZPP1 (100 µl of of 500 µM solution in PBS) was intravenously injected. After 30 min from the injection, skin and peritoneum incision was carefully made to expose seminal vesicle and prostate without damaging blood vessels. Several drops of saline water pre-warmed to 37 °C were applied and a cover slip was placed on the exposed tissue to avoid dehydration. After each imaging session, mice were either sacrificed for histological analysis or saved for longitudinal study at a later time point by closing the incised skin and peritoneum with 6-0 nylon suture and applying triple antibiotic ointment. Fluorescence signals of ZPP1 were obtained by excitation with a 491nm continuous wave (CW) laser (Dual-Calypso, Cobolt, Sweden) and detections by photomultiplier tubes (R9110, Hamamatsu, Japan) through 520 ±17nm (ZPP1) and 579 ±17nm (autofluorescence) band pass filters (Semrock, Inc., Rochester, NY). Post-image processing and 3D reconstruction were performed by ImageJ and Matlab, respectively.

Histology.

After in vivo imaging, the prostate was excised, embedded in Tissue-Tek O.C.T. Compound (Sakura Fineteck, Japan), and snap-frozen in liquid nitrogen. Twenty-μm sections were prepared and fixed in 4% formaldehyde for 5 min. The slides were mounted in Vectashield mounting medium with DAPI (Vector Laboratories, Burlingame, CA) and visualied by fluorescence microscopy as described above. Consecutive sections were stained with hematoxylin & eosin (H&E) and analyzed by light microscopy for histopathology.

Statistical Analysis

Data were expressed as means ± SDs. Statistical differences were analyzed by a two-tailed t-test (SigmaStat 3.0; Systat Software, Richmond, CA). A value of $P < 0.05$ was taken as statistically significant.

Results

Zinc Sensing in Cell Culture Using ZPP1

Before embarking on in vivo studies we had to establish the utility of zinc sensing using ZPP1 in cancerous and normal prostate cell lines. Normal (RWPE1) and transformed (RWPE2) human prostate epithelial cells were analyzed by fluorescence microscopy (Fig. 1A) following treatment with ZPP1. Treatment with ZPP1 resulted in bright fluorescence in the normal RWPE1 cells (Fig. 1A) with significant extranuclear distribution of the signal (Suppl. Fig. 1), which was quenched by subsequent application of the extracellular zinc ion chelator tris(2-pyridyl)amine (TPA). This effect is consistent with the uptake of extracellular zinc by the cells through one or more of several plasma membrane transporters such as ZIP1 (4). By contrast, the signal associated with the transformed RWPE2 cells in which the ZIP1 transporter is downregulated ((4) and Fig. 1C) was considerably lower, indicative of overall reduced levels of zinc uptake (Fig. 1A). This difference was also visible in cells incubated with culture media without added $ZnCl_2$, consistent with the presence of small amounts of zinc in the media (Fig. 1A). Flow cytometry measurements of ZPP1 turn-on fluorescence confirmed the presence of zinc in normal prostate cells and the reduced zinc uptake by transformed RWPE2 cells (Fig. 1B). As also shown by fluorescence microscopy, addition of TPA reduced the fluorescence intensity in both cell lines to background levels (Fig. 1B), indicating that the detected zinc was intracellular.

Finally, to quantify the difference in actual zinc concentrations in normal and transformed prostate adenocarcinoma cell lines we obtained lysates from RWPE1 and RWPE2 cells and performed a ZPP1 titration assay, as described previously (10). The

biphasic response of ZPP1 to zinc allowed us to accurately determine the concentration of mobile zinc in the cell lysates. From the ZPP1 concentration at maximum fluorescence on the titration curve (Fig. 1D) following overnight incubation with $ZnCl_2$ (50 μM) and using the relationship

$$[ZPP1]_{max} = 0.5[Zn^{2+}]$$

we estimated an intracellular mobile zinc level of 12-16 fmol per cell in the RWPE1 cell line, which was consistent with the literature (22). Mobile zinc in the RWPE2 cells was estimated in a similar manner to be 6-8 fmol per cell (Fig. 1D). This difference in cellular mobile zinc levels in these cells correlated with the total zinc concentrations as measured by inductively coupled plasma-mass spectrometry (ICP-MS; RWPE1: 20±0.2; RWPE2: 9±0.4 fmoles/cell), supporting the validity of our observations. In order to further corroborate the reduced zinc content in prostate cancer cells and the suitability of ZPP1 as a sensor for its detection, we analyzed LNCaP and DU145 human prostatic adenocarcinoma representing androgen-dependent and androgen-independent variants of advanced disease respectively. Fluorescence microscopy revealed virtually no zinc sensing in the presence of added zinc and ZPP1 (Suppl. Fig. 2A). ZPP1 titrations (Suppl. Fig. 2B) of lysates from both cell lines showed undetectable mobile zinc levels, as indicated by the absence of a single distinct peak in the fluorescence titration curves. These results are consistent with the low total zinc concentration of the cell lines, measured by ICP-MS (RWPE1: 20±0.2; LNCaP: 3±0.1; DU145: 3±0.3 fmoles/cell). These initial in vitro findings demonstrated the utility of ZPP1 as a sensor to distinct zinc

concentrations in normal and cancerous prostate cells.

In Vivo Prostate Imaging with ZPP1

As a first step toward demonstrating the feasibility of detecting prostate cancer in vivo using ZPP1 as a fluorescent reporter, we imaged the prostate of healthy C57BL/6J mice. At 30-min after intravenous injection, there was bright fluorescent signal associated with the area of the prostate, which was not present prior to the injection of the dye (Fig. 2A). To demonstrate that this signal was zinc-specific, we co-injected a cohort of mice with ZPP1 and a 10-fold excess of the zinc chelator TPA. As a result of this treatment the fluorescent signal was reduced to background levels ($p = 0.01$, $n = 4$; Fig. 2A and B), confirming the specificity of ZPP1 for zinc sensing in vivo. To assure that the observed fluorescence signal was derived from the prostate, in a subset of animals we performed transillumination optical imaging with tomographic reconstruction. The origin of the fluorescence signal was located dorsally to the urinary bladder and posteriorly to the kidneys, consistent with the anatomic location of the prostate (Suppl. Movie 1). Ex vivo imaging of excised prostates of mice injected with ZPP1 alone displayed bright fluorescence. Only diffuse background fluorescence was observed in prostates from the mice co-injected with TPA (Fig. 2C). Histological analysis of frozen prostate sections from these mice confirmed the zinc-specific, ZPP1-mediated signal enhancement, which was mostly associated with the glandular compartment (Fig. 2D).

This observation was confirmed by intravital microscopy, which showed that the signal 30 min after injection was associated with the zinc-rich prostatic glandular epithelium following initial enhancement of the local microvasculature (Fig. 3A).

To address the issue of potential confusion between prostate signal and signal

from the bladder we imaged both organs after intravenous injection of ZPP1 in vivo. As shown in Figure 3B, there was minimal enhancement of the bladder compared to the prostate. This finding, together with tomographic reconstruction identifying the location of the prostate (Suppl. Movie 1), assured us of the capability of ZPP1, as a turn-on fluorescent agent, to specifically detect zinc in the prostate.

In Vivo Prostate Cancer Detection and Monitoring

Having established that our method can be applied for the detection of prostatic zinc in vivo and that ZPP1 is sensitive to the reduced zinc content of cancer cells, we evaluated the potential of this probe to monitor prostate cancer progression in transgenic adenocarcinoma of the mouse prostate (TRAMP, C57BL/6-Tg(TRAMP)8247Ng/J) mice (Jackson Laboratory, Bar Harbor, ME). This strain exhibits prostatic epithelial neoplasia (PIN) by 12 weeks of age, whereas tumors, appearing as well differentiated adenocarcinoma, can arise by 24 weeks of age, mostly in the dorsal and lateral lobes of the prostate. The development of prostate cancer in this model resembles the human condition and is broadly accepted by prostate cancer researchers (12).

We imaged male TRAMP mice by noninvasive epi-fluorescence optical imaging, beginning at 15 weeks of age and until 28 weeks of age, in order to cover the spectrum from early to advanced localized disease. We observed a loss of fluorescence signal with disease progression beginning at 19 weeks of age, which is the age representative of well-differentiated localized carcinoma (Fig. 4A) but not at 15 weeks of age, when the animals displayed PIN (Fig. 4C). By 28 weeks of age, the signal associated with the TRAMP prostate was reduced twofold, compared to healthy age-matched controls ($p = 0.02$, $n = 4$; Fig. 4A).

These observations were confirmed by ex vivo optical imaging (Fig. 4B). Whereas in the healthy animals the prostate remained brightly fluorescent across all ages, in the TRAMP animals, there was a visible loss of signal with age, reflective of reduced zinc levels (Fig. 4B). Histopathological analysis of TRAMP prostates revealed the presence of only PIN at 15 weeks of age, well-differentiated carcinoma at 19 weeks of age, and progressive disorganization of the glandular epithelium with the transition to moderately (24 weeks) and poorly (28 weeks) differentiated cancer. By contrast, the glandular organization was preserved in the C57BL/6J controls, even at 28 weeks of age (Fig. 4C). Fluorescence microscopy of prostate tissue from mice injected with ZPP1 demonstrated that our agent could be used to define the disruption of the glandular architecture and reduction in zinc content in the TRAMP animals (Fig. 4C). To confirm the reduced zinc content in the prostate of 28-wk old TRAMP mice compared to C57BL/6J healthy mice, we measured zinc levels in tissue extracts by ZPP1 titration, in the manner employed by our in vitro studies (Fig. 4D). The mobile reactive zinc level in extracts from the TRAMP prostates, measured by the titration method, was not detectable. By contrast, zinc concentration in the prostate of healthy mice was 194±24 nmol/g of tissue (Fig. 4D). The reduction in *mobile* zinc content translated into a decrease of *total* zinc content, as measured by ICP-MS. There was a three-fold reduction in the weight-adjusted total zinc content of the TRAMP vs. C57BL/6J prostates ($p = 0.003$, $n = 2$). Combined, these results revealed that there was a dramatic reduction of zinc levels in the tumors accompanying cancer progression and that this trend could be detected by in vivo imaging with ZPP1.

Intravital microscopy confirmed a loss of fluorescence signal with disease progression, which was evident even at 16 weeks of age, consistent with the superior spatial resolution of this method and its sensitivity to local variations in zinc content (Fig. 5 and Suppl. Movie 2, 3, and 4). These results were not seen in age-matched C57BL/6J animals, in which the epithelial cell layer remained well organized and rich in zinc even at 28 weeks of age.

Importantly, the observed reduction in prostatic zinc content was characteristic of cancer. No decrease in prostate-derived fluorescence was observed in a model of inflammation (Suppl. Fig. 3A and B), which was confirmed by the presence of substantial mononuclear cell infiltration (Suppl. Fig. 3C). The sustained prostatic zinc content in this model of inflammation was confirmed by ICP-MS ($p > 0.05$, $n = 2$).

Discussion

Prostate cancer is a highly prevalent disease, for which there is no cure once it is no longer organ-confined. In spite of the controversy in the clinical and scientific communities surrounding the need for prostate cancer testing, recent trials have affirmed the life-saving value of early diagnosis, especially in younger men (23). Considering that according to the American Cancer Society, 1 in 35 men in the U.S. will die of prostate cancer, there should be no debate about the need for an effective and reliable diagnostic tool for early detection as a facilitator of successful therapy.

In response to this need, we have demonstrated the value of in vivo imaging and quantitation of zinc as a reliable biomarker for prostate cancer using our novel fluorescent probe ZPP1. One of its key advantages over screening for serum PSA is that, whereas PSA is elevated in both cancer and BPH, zinc levels are drastically reduced in prostate cancer (6). Therefore, monitoring levels of zinc in the prostate can resolve the ambiguity of the PSA test in discriminating between BPH and cancer, which is probably the most critical element confounding diagnosis, considering that the majority of men in the high-cancer over 55 age group will develop BPH.

. The studies presented here describe a new diagnostic method, taking advantage of the special properties of the zinc-sensitive fluorescent agent ZPP1. This probe is quantitative, potentially less ambiguous, and considerably more sensitive and specific for the detection of prostate cancer than existing modalities. Specific advantages of ZPP1 include high accuracy, high zinc selectivity, low-cost, and ease of utilization for zinc detection and quantification. As shown through our studies, the unique two-step fluorescence response manifest by ZPP1 allows accurate quantitation of mobile zinc

concentrations in biological samples (cell and tissue lysates) by simple titration of the agent.

In addition, the specific turn-on fluorescence response of ZPP1 to zinc and the suitability of the agent for in vivo delivery, as demonstrated in our animal experiments, allowed us to visualize the zinc-rich prostate by fluorescence optical imaging and to monitor the zinc depletion of the organ during the development of prostate cancer. We utilized both noninvasive whole-body optical imaging and an intravital microscopic approach. While the former has not been yet fully introduced into the clinic, the latter may gain significance having in mind the increasing clinical relevance of endoscopic optical imaging. Our results suggested the possibility to develop a very specific and sensitive clinical tool for prostate cancer detection and monitoring based on a method similar to endomicroscopy. One can envision a scenario in which an optical probe is positioned in immediate proximity to the prostate and the tissue is examined at microscopic resolution. The unique advantage of this method, as demonstrated by our results, is the ability to examine the tissue at a cellular level, with high contrast and, therefore, potentially to detect very early lesions.

Overall, the described studies clearly illustrate the value of zinc-based prostate-cancer diagnostics, as suggested through years of prior research (6). However, to our knowledge, this is the first study that utilized zinc as an imaging biomarker for prostate cancer progression. The methods that we have developed can be used separately or in combination as a preclinical or clinical tool.

Acknowledgements

We thank Pamela Pantazopoulos (Molecular Imaging Laboratory, Martinos Center for Biomedical Imaging, MGH) for help with the in vitro assays, Marytheresa Ifediba for help with the animal studies, Dr. Daniela Buccella (MIT) for materials, and Drs. Ritika Uppal, Galen Loving, and Peter Caravan (Martinos Center for Biomedical Imaging, MGH) for help with ICP-MS. Confocal microscopy was performed at the Confocal Microscopy Core at MGH with technical assistance from Igor A. Bagayev, M.S.

References

1. Jemal A, Murray T, Ward E, et al. Cancer statistics, 2005. CA Cancer J Clin 2005; 55: 10-30.

2. Fitzsimons NJ, Sun L, Moul JW. Medical technologies for the diagnosis of prostate cancer. Expert Rev Med Devices 2007; 4: 227-39.

3. Nash AF, Melezinek I. The role of prostate specific antigen measurement in the detection and management of prostate cancer. Endocr Relat Cancer 2000; 7: 37-51.

4. Franklin RB, Feng P, Milon B, et al. hZIP1 zinc uptake transporter down regulation and zinc depletion in prostate cancer. Mol Cancer 2005; 4: 32.

5. Mawson CA, Fischer MI. The occurrence of zinc in the human prostate gland. Can J Med Sci 1952; 30: 336-9.

6. Costello LC, Franklin RB. Prostatic fluid electrolyte composition for the screening of prostate cancer: a potential solution to a major problem. Prostate Cancer Prostatic Dis 2009; 12: 17-24.

7. Zaichick VY, Sviridova TV, Zaichick SV. Zinc concentration in human prostatic fluid: normal, chronic prostatitis, adenoma and cancer. Int Urol Nephrol 1996; 28: 687-94.

8. Cortesi M, Chechik R, Breskin A, et al. Evaluating the cancer detection and grading potential of prostatic-zinc imaging: a simulation study. Phys Med Biol 2009; 54: 781-96.

9. Cortesi M, Fridman E, Volkov A, et al. Clinical assessment of the cancer diagnostic value of prostatic zinc: a comprehensive needle-biopsy study. Prostate 2008; 68: 994-1006.

10. Zhang XA, Hayes D, Smith SJ, Friedle S, Lippard SJ. New strategy for quantifying biological zinc by a modified zinpyr fluorescence sensor. J Am Chem Soc 2008; 130: 15788-9.

11. Chin AI, Miyahira AK, Covarrubias A, et al. Toll-like receptor 3-mediated suppression of TRAMP prostate cancer shows the critical role of type I interferons in tumor immune surveillance. Cancer Res; 70: 2595-603.

12. Greenberg NM, DeMayo F, Finegold MJ, et al. Prostate cancer in a transgenic mouse. Proc Natl Acad Sci U S A 1995; 92: 3439-43.

13. Bai A, Higham E, Eisen HN, Wittrup KD, Chen J. Rapid tolerization of virus-activated tumor-specific CD8+ T cells in prostate tumors of TRAMP mice. Proc Natl Acad Sci U S A 2008; 105: 13003-8.

14. Niu Y, Altuwaijri S, Yeh S, et al. Targeting the stromal androgen receptor in primary prostate tumors at earlier stages. Proc Natl Acad Sci U S A 2008; 105: 12188-93.

15. Luo JL, Tan W, Ricono JM, et al. Nuclear cytokine-activated IKKalpha controls prostate cancer metastasis by repressing Maspin. Nature 2007; 446: 690-4.

16. Drake CG, Doody AD, Mihalyo MA, et al. Androgen ablation mitigates tolerance to a prostate/prostate cancer-restricted antigen. Cancer Cell 2005; 7: 239-49.

17. Hurwitz AA, Foster BA, Kwon ED, et al. Combination immunotherapy of primary prostate cancer in a transgenic mouse model using CTLA-4 blockade. Cancer Res 2000; 60: 2444-8.

18. Gingrich JR, Barrios RJ, Kattan MW, Nahm HS, Finegold MJ, Greenberg NM. Androgen-independent prostate cancer progression in the TRAMP model. Cancer Res 1997; 57: 4687-91.

19. Ellwood-Yen K, Graeber TG, Wongvipat J, et al. Myc-driven murine prostate cancer shares molecular features with human prostate tumors. Cancer Cell 2003; 4: 223-38.

20. Corbacho AM, Valacchi G, Kubala L, et al. Tissue-specific gene expression of prolactin receptor in the acute-phase response induced by lipopolysaccharides. Am J Physiol Endocrinol Metab 2004; 287: E750-7.

21. Kim P, Puoris'haag M, Cote D, Lin CP, Yun SH. In vivo confocal and multiphoton microendoscopy. J Biomed Opt 2008; 13: 010501.

22. Costello LC, Liu Y, Zou J, Franklin RB. Evidence for a zinc uptake transporter in human prostate cancer cells which is regulated by prolactin and testosterone. J Biol Chem 1999; 274: 17499-504.

23. Lin DW, Porter M, Montgomery B. Treatment and survival outcomes in young men diagnosed with prostate cancer: a Population-based Cohort Study. Cancer 2009; 115: 2863-71.

Figure Legends

Figure 1. In vitro studies. (A) Fluorescence microscopy of RWPE1 and RWPE2 cells following (from left to right) sham treatment, incubation with ZPP1 in the absence of zinc chloride, incubation with ZPP1 in the presence of added zinc chloride, and incubation with ZPP1 in the presence of added zinc, followed by a total zinc chelator (TPA). **(B)** Flow cytometry raw histogram (top) and quantification (bottom) of RWPE1 and RWPE2 cells following sham treatment, incubation with ZPP1 in the absence of zinc, incubation with ZPP1 in the presence of added zinc, and incubation with ZPP1 in the presence of added zinc, followed by a total zinc chelator (TPA), as described in (a). **(C)** Confocal microscopy of RWPE1 and RWPE2 cells following immunostaining with ZIP1-specific antiserum. The differences in zinc uptake between the two cell lines extended from differences in the expression levels of the ZIP1 zinc transporter. Results are representative of at least three independent experiments. **(D)** Determination by ZPP1 titration of mobile zinc concentration in cell lysates derived from RWPE1 and RWPE2 cells incubated with a 50 μM concentration of $ZnCl_2$. The results represent a summary of two independent experiments.

Figure 2. In vivo detection of zinc in the mouse prostate by epi-fluorescence whole-body optical imaging. (A) Noninvasive, whole-body epi-fluorescence optical imaging of C57BL/6J mice before (left) and 30 min after (right) tail-vein injection of ZPP1 alone (top) or ZPP1 plus TPA (bottom). There was a strong signal enhancement associated with the area of the prostate after injection of ZPP1 in the absence of chelator, indicating specific detection of zinc. **(B)** Quantitative evaluation of the results illustrated in (A), reflecting relative fluorescence efficiency derived from a region of interest around the

area of the prostate. There was an increase in normalized efficiency in the mice injected with ZPP1, which was significantly higher than in mice co-injected with chelator ($p = 0.01$; $n = 4$), suggesting specific detection of zinc. Fluorescence efficiency derived from the area of the prostate was represented as a fraction of that in adjacent muscle tissue. **(C)** Ex vivo epi-fluorescence optical imaging of the prostate and seminal vesicles (left) and adjacent muscle tissue (right) of C57BL/6J mice 30 min after tail-vein injection of ZPP1 alone (top) or ZPP1 plus TPA (bottom). **(D)** Fluorescence microscopy of frozen prostatic tissue sections derived from non-injected C57BL/6J mice (left), mice injected with ZPP1 alone (green, middle), or ZPP1 plus chelator (right). In the ZPP1-injected group, there was a visible fluorescence enhancement of the glandular regions of the tissue, which was not seen in non-injected mice and was dramatically reduced upon co-injection with chelator. Cells were co-stained with DAPI (blue) for nuclear detection.

Figure 3. In vivo detection of zinc in the mouse prostate by intravital microscopy. **(A)** Imaging (from left to right) pre-injection, 1 min, and 30 min after intravenous injection of ZPP1 (green). Examination of the prostate tissue before injection of ZPP1 revealed a low level of autofluorescence (left). Immediately after injection of the imaging agent (1 min), there was a clear enhancement of the local microvasculature (arrow) and the prostatic glandular epithelium (arrowhead), surrounding the glandular lumen (L). Imaging at 30 min post-ZPP1 injection demonstrated a very prominent enhancement of the glandular regions. **(B)** Distribution of ZPP1 fluorescence in mouse prostate and bladder. The majority of ZPP1 fluorescence after in vivo delivery was found in the prostatic epithelium. The bladder demonstrated minimal enhancement, following injection of the imaging agent.

Figure 4. In vivo detection and monitoring of prostate cancer by epi-fluorescence whole-body optical imaging. **(A)** Noninvasive, whole-body epi-fluorescence optical imaging of 15-, 19-, 24-, and 28-wk old TRAMP (bottom) and C57BL/6J (top) mice 30 min after tail-vein injection of ZPP1. In the TRAMP mice, consistent with prostate cancer progression, there was an overall reduction in prostate-associated fluorescence with age, beginning at 19 weeks of age. By contrast, the signal in the C57BL/6J mice remained the same (n = 4). Fluorescence efficiency relative to muscle tissue was normalized to 1. **(B)** Ex vivo epi-fluorescence optical imaging of the prostate (P), seminal vesicles (SV) and adjacent muscle tissue (M) of TRAMP (bottom) and C57BL/6J (top) mice injection of ZPP1. There was a strong signal enhancement of the prostate in both groups at 15-wks of age. In the TRAMP mice, there was an overall reduction in the prostate-associated signal with age (24 wks is shown). By contrast, the signal in the C57BL/6J mice remained the same **(C)** Histopathology (top) and fluorescence microscopy (bottom) of prostatic tissue sections derived from 15-, 19-, 24-, and 28-wk old TRAMP and 28-wk old C57BL/6J mice injected with ZPP1. Note the progressive disorganization of the glandular epithelium with age in the prostates of TRAMP mice. By contrast, the glandular organization was preserved in the C57BL/6J controls, even at 28 wks of age. Fluorescent images are represented as an overlay of the green (ZPP1) and ultraviolet (DAPI, blue) channels. (**D**) Quantitation of zinc concentrations by ZPP1 titration in prostatic tissue extracts derived from 28-wk old TRAMP and C57BL/6J mice. The results represent a summary of two independent experiments.

Figure 5. Confocal intravital microscopy of prostate cancer progression. Intravital confocal microscopy 30 min after intravenous injection of ZPP1 (was performed at 16-,

20-, 24-, and 28-wks of age. In TRAMP mice (bottom), loss of tissue zinc content was seen even at 16 wks of age. There was a progressive loss of fluorescence and disorganization of the zinc-positive epithelial cell layer with age. This result was not obtained in the age-matched C57BL/6J controls (top), in which the epithelial cell layer remained well organized and rich in zinc even at 28 wks of age.

Medarova Figure 1

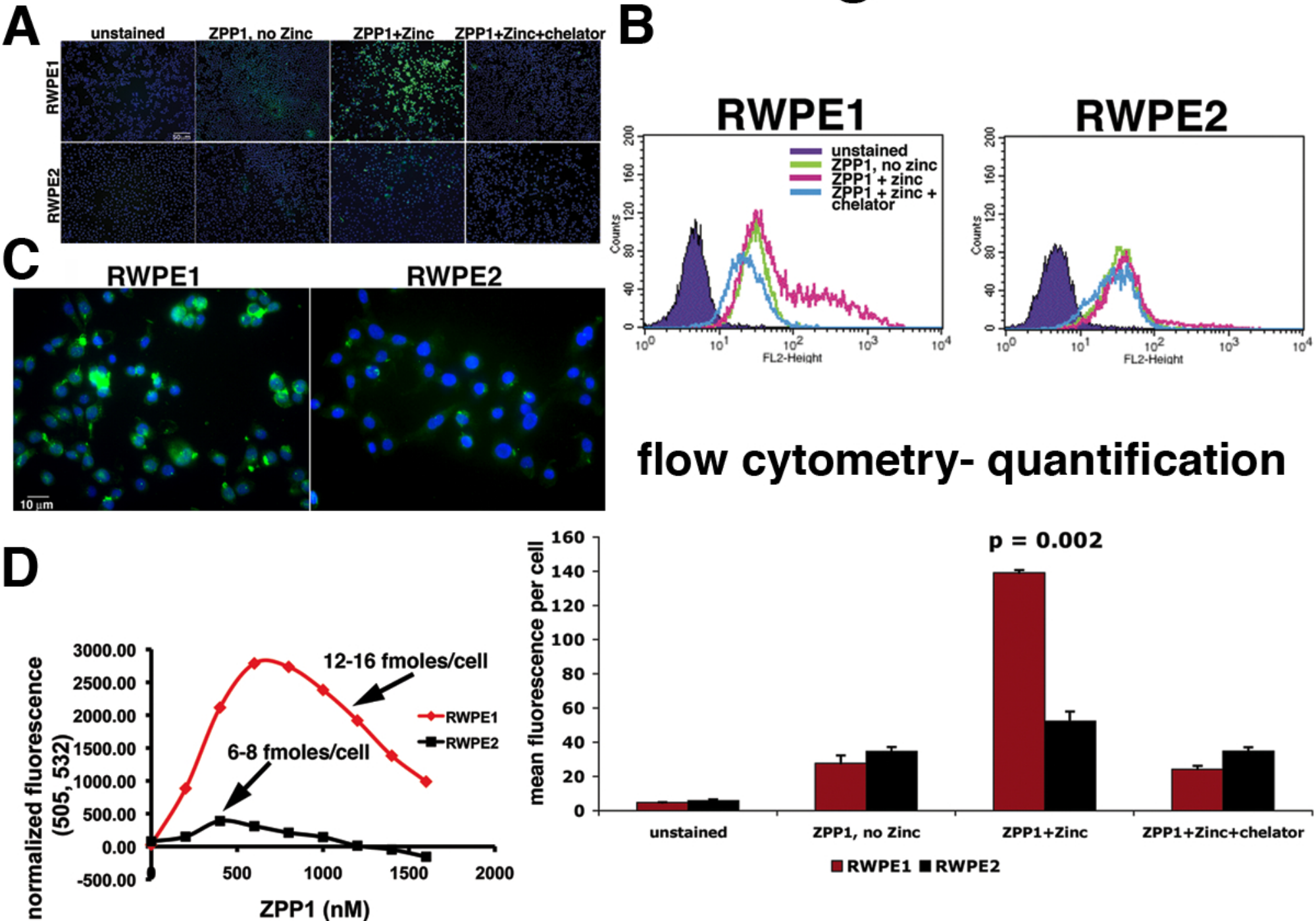

Medarova Figure 2

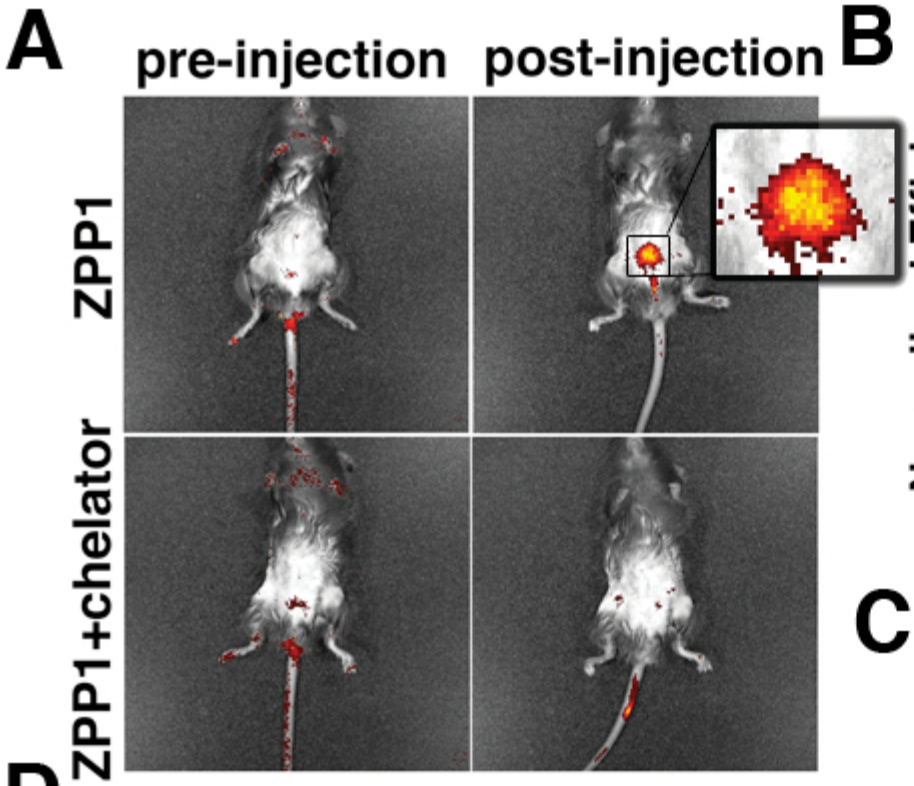

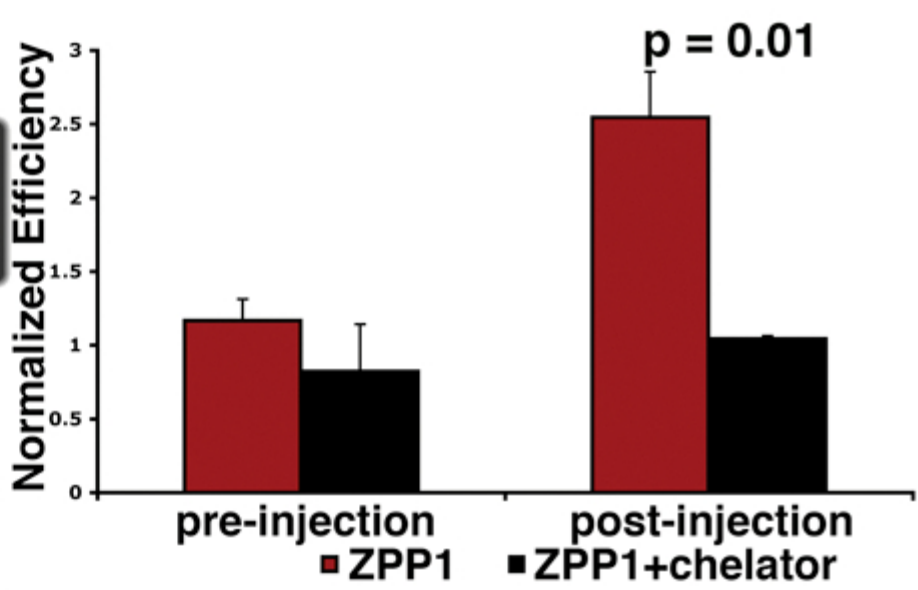

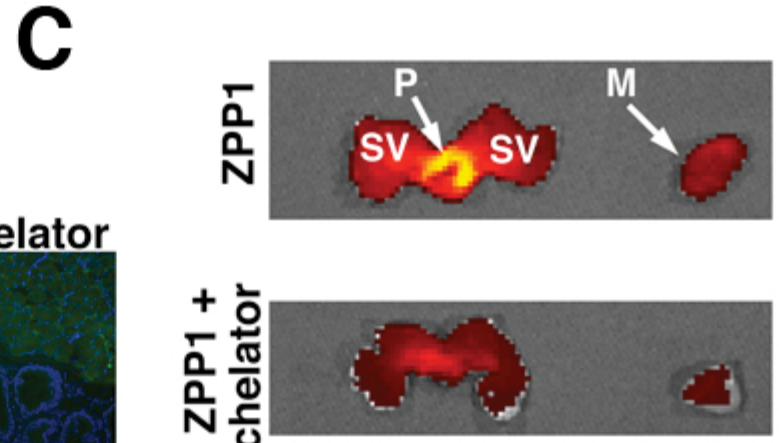

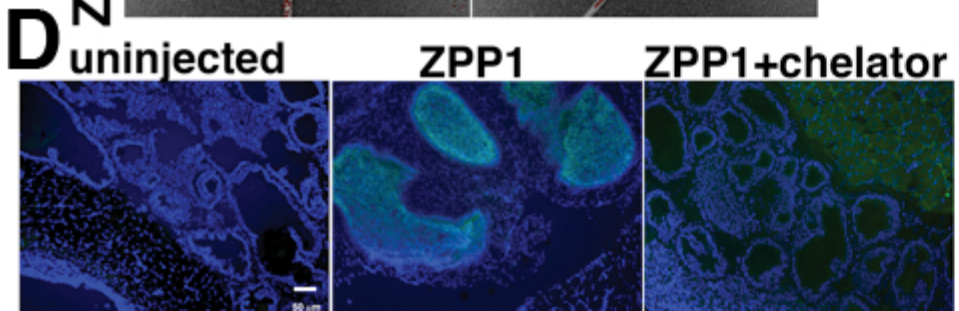

Medarova Figure 3

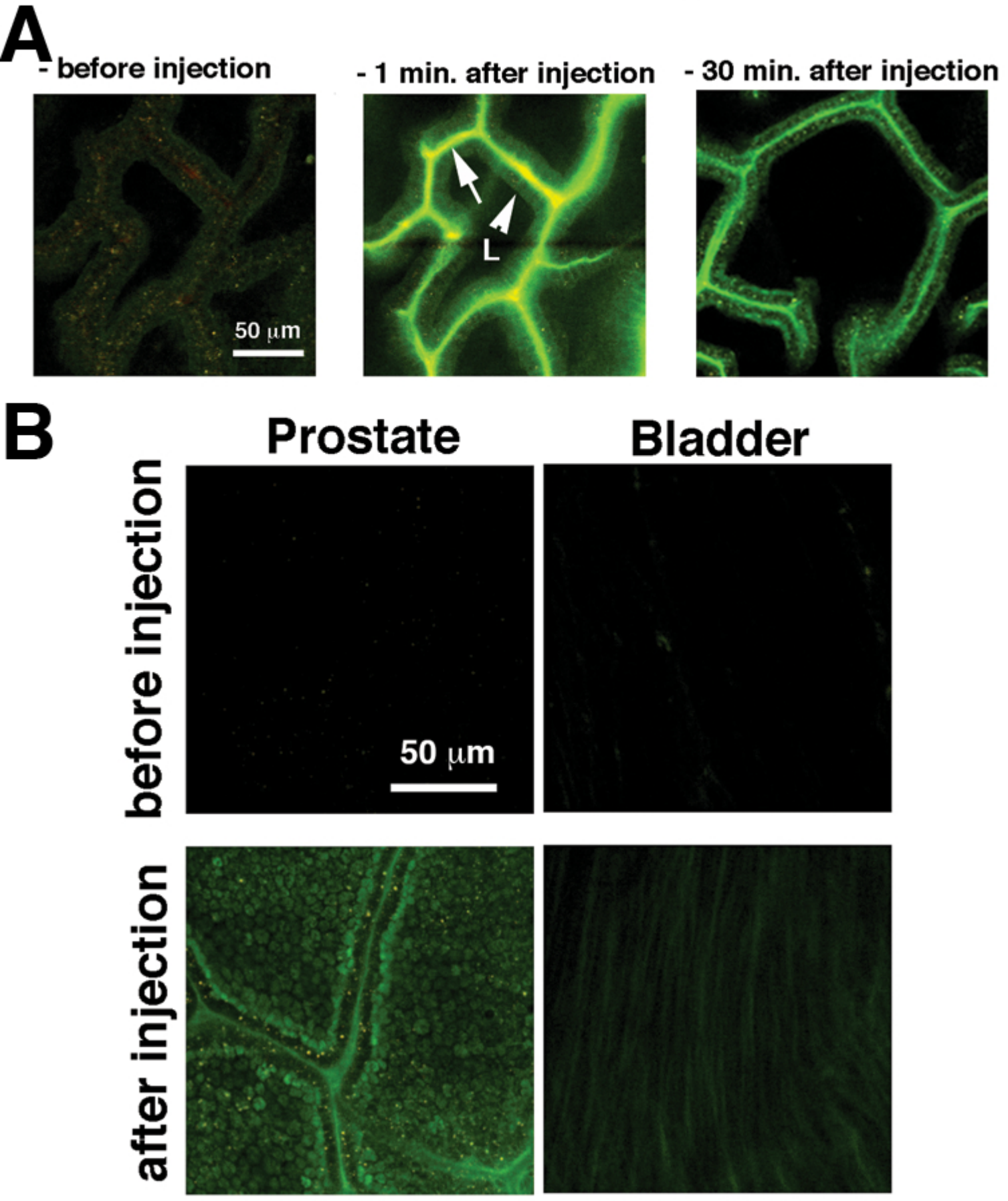

Medarova Figure 4

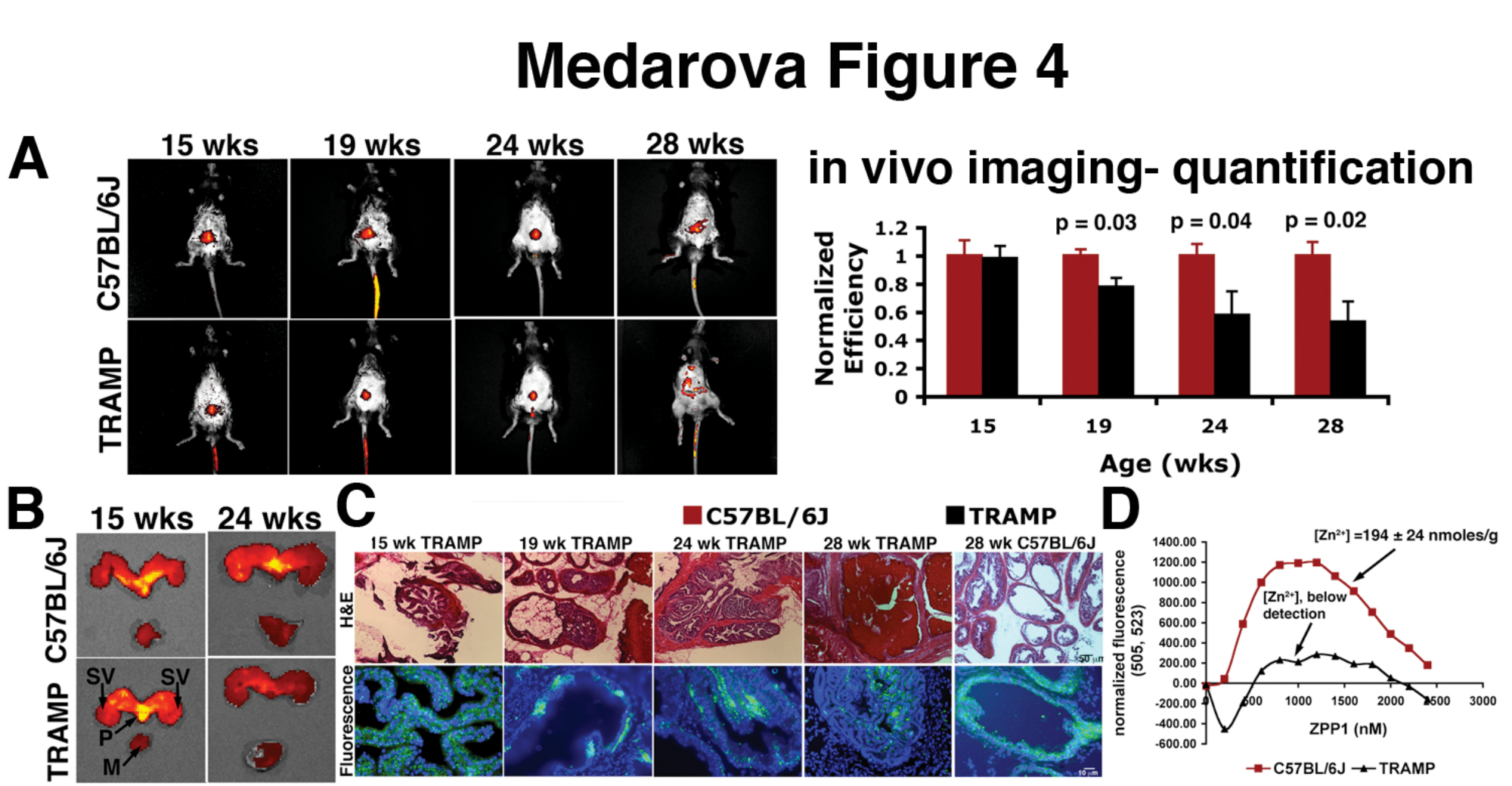

Medarova Figure 5